# Delta-range coupling between prefrontal cortex and hippocampus supported by respiratory rhythmic input from the olfactory bulb

Rola Mofleh and Bernat Kocsis

Dept Psychiatry at BIDMC, Harvard Medical School
Correspondence: bkocsis@hms.harvard.edu

**Abstract**
Respiratory rhythm (RR) during sniffing is known to couple with hippocampal theta rhythm. However, outside of the short sniffing bouts, a more stable ~2Hz RR was recently shown to rhythmically modulate non-olfactory cognitive processes, as well. The underlying RR coupling with wide-spread forebrain activity was confirmed using advanced techniques, including current source density and phase modulation of local gamma activity, creating solid premise for investigating how higher networks use this mechanism in their communication. Here we show essential differences in the way prefrontal cortex (PFC) and hippocampus (HC) processes the RR signal from the olfactory bulb (OB) allowing dynamic PFC-HC coupling utilizing this input. We found stable OB-PFC coherence in waking contrasting low but highly variable OB-HC coherence. PFC-HC coupling however primarily correlated with the latter, indicating that HC access to the PFC output readily segmented and shaped by RR in the delta range is dynamically regulated by the responsiveness of HC to the common rhythmic drive.

## 1. Introduction

More than half a century after the first observations[1], an explosion of recent findings firmly demonstrates that brain activity and cognitive function in rodents and humans are modulated synchronously with nasal respiration (rev.[2]). Respiratory related oscillations (RRO) were detected in numerous brain structures, including higher order cognitive centers in the prefrontal cortex (PFC)[3, 4] and hippocampus (HC)[5-7]. Respiratory rhythm primarily derived from rhythmic nasal airflow by the olfactory bulb (OB)[6] dynamically couples with intrinsic network oscillations in these structures either by coherence, when the frequency of RRO matches that of local field potentials (LFP), e.g. in the delta and theta ranges in rodents[3, 5-9], or by phase-amplitude modulation when the frequencies diverge, e.g. gamma in rodents[3, 4, 6, 8] and most components of the human EEG, relevant for cognitive function (delta, theta, alfa, gamma)[10].

New evidence rapidly accumulating in the past decade extended research on the mechanisms of OB-cortical RRO coupling well studied in sniffing episodes to those associated with continuous on-going respiration raising questions of how RRO may be involved in non-olfactory cognitive processing[11, 12]. Respiratory modulation of a wide range of cognitive functions was reported both in rodents and human, from sensory processing and motor coordination to a variety of memory functions (rev.[12]), not directly related to olfaction or the primary respiratory function of gas exchange. Rhythmic coupling is a powerful ubiquitous mechanism of functional coordination of neural ensembles and RRO appears to provide a potential carrier for such synchronization with a wide, perhaps even global[2, 9], access to various networks, cortical as well as subcortical. For functional networks, this access has to be dynamically regulated in a state and task dependent manner to include specific circuits involved in certain tasks when it is necessary and uncouple when it is not. The anatomical substrate of carrying the RRO signal to different networks may be suitable for such control. RRO from different sources[13], of which OB is dominant, is transmitted by diverse multi-synaptic pathways whereas different networks may synchronize with this input in different ways, determined by their unique circuit characteristics and connectivity. For example, key intrinsic oscillations in PFC (delta, 2-5 Hz[14-16]) are in the range of on-going RRO whereas in HC they are faster (theta, 5-10 Hz[17]), overlapping in rodents with sniffing RRO frequency. These two forebrain structures are the focus of the current study investigating how the RRO signal generated in the OB may potentially contribute to PFC-HC communication by synchronizing their activities at the respiratory rate.

Effective PFC-HC communication is important for normal cognition and impaired PFC-HC coupling was implicated in cognitive deficits in psychiatric diseases[18-21]. We have shown recently by studying forebrain oscillations induced by the ascending arousal input from brainstem in urethane anesthetized rats that rhythmic coupling between PFC and HC can be established in both delta and theta ranges, even simultaneously, and proposed that they may serve as parallel channels of communication in opposite directions between the two structures[22]. RRO and theta was also shown to co-exist in chronic experiments during theta states with an asymmetric regional distribution of RRO dominant in the frontal and theta in more caudal cortical areas[9]. Based on these data we hypothesized that RRO might enhance the communication between distant PFC and HC networks primarily in the PFC-to-HC direction. Correlation between RRO coherences through the OB, i.e. maintained with diaphragmal (dia) EMG on one hand and forebrain LFPs on the other, revealed a strong faithful RRO transmission to PFC whereas OB-HC coherence was lower and did not necessarily follow the RRO input to OB. Although weak on average, OB-HC coherence was highly variable, however, and showed strong correlation with PFC-HC RRO coherence indicating that HC access to the PFC output readily segmented and shaped by the RRO in the delta range is dynamically regulated by the responsiveness of HC to the common RRO

drive. The details of this regulation remain unknown as our recordings were performed in undisturbed conditions, limited to spontaneous behaviors and different sleep-wake states. We found however that this pattern was only present in waking, both theta and non-theta states, whereas PFC-HC communication appeared protected from RRO synchronization in sleep states.

## 2. Methods

Eighteen adult, male rats (360–560g, Charles River Laboratories) were used in this study. Experiments were performed on 10 rats under urethane anesthesia, whereas the remaining 8 rats were subjected to survival surgery followed by chronic recordings in free behaviors. All procedures were performed in accordance with the Institutional Animal Care and Use Committee of Beth Israel Deaconess Medical Center.

**2.1. Anesthetized rats** Urethane (i/p; 1.2-1.5 g/kg of 65-80% solution) was given in two doses, an hour apart with ketamine supplemented (3.5 to 5 mg/kg) if necessary by monitoring reaction to tail pinch. The body temperature was maintained by isothermal pad. First, a 10 mm cut was made on the right side of the abdomen through which the diaphragm was palpated with the edge of the forceps to find the right position for implantation of the electrodes. Two multi-threaded electrode wires were implanted and fixed with surgical glue for recording of the EMG. The incision was closed by 5-6 sutures. The dia electrodes were tunneled under the skin up to the skull.

The second part of the surgery was performed in a stereotaxic frame, where the recording electrodes were implanted according to the Atlas of Paxinos[23]. Stainless steel screw above the parietal cortex (AP: -3.5 mm, Lat: 2.5 mm from bregma) was inserted on the left side to record the cortical EEG, two screws were inserted in the nasal bone (~5.0 mm anterior to bregma) and above the cerebellum to act as reference and ground electrodes. Two single electrodes (stainless steel wires) were implanted on each side (AP: +3.2 mm, Lat: ±0.5 mm, DV: -5.1 mm) to record the electrical activity in the PFC, a single electrode on the left side for the OB (AP: +8.5 mm, Lat: 1.5 mm, DV: -1.6 mm), and a pair of twisted wires with 1 mm between their tips in the HC on the right side (AB: -3.7, Lat: 2.2 mm, DV: -3.5 mm) (Fig. S1). All the electrode wires and screws were fixed to the skull with dental acrylic. The electrodes were connected to an amplifier (A-M systems) for data recording, filtered between 0.3 and 100 Hz, whereas the dia EMG filters had both low- and high-pass filters set at 100 Hz to diminish unwanted noise including respiratory movement artifacts and electrical noise from the heart (Fig. S2). The local field potentials (LFP) were recorded and saved in DASYLab 7.0 Acquisition System. When a sufficient amount of data was collected, approximately around one hour, the rats were euthanized by injection of Ketamine, 1 ml.

**2.2. Chronic experiments** Survival surgeries were conducted on 8 rats under sterile conditions. Deep anesthesia was maintained by Ketamine-Xylazine mixture (i/p; 30-40 mg/kg ketamine and 5 mg/kg Xylazine) with supplementary injections of Ketamine (10 % of the initial dose) if necessary. The electrodes were implanted as described above. In addition, two multi-threaded electrodes in soft insulation were implanted in the neck muscles on each side to evaluate general motor activity and tone to identify states, such as sleep and exploration. Antibiotic gel was applied before suturing the incisions. Meloxicam analgesics, 1 mg/kg of 5 mg/ml daily, was given subcutaneously two days in a row to relieve pain. The rats were observed until they fully woke up. They recovered for a week in their home cages before the first 24 hours-recording. These recordings included different behaviors and sleep-wake states while the rat was freely moving in the cage, undisturbed. The rats were euthanized by 1 ml of Ketamine injections 3 weeks later and the brains were extracted for verification of the electrode position (Fig. S1).

**2.3. Data and statistical analysis** In two 24 hr recordings, acquired a couple of days apart in each rat, sleep-wake states were identified using standard criteria based on cortical EEG, HC LFP, and neck muscle EMG recordings. In waking, characterized by high and variable muscle activity, active waking (AW) and quiet waking (QW) were separated by the presence or absence, respectively, of HC theta rhythm and low amplitude fast cortical EEG. Sleep periods, characterized by continuously low muscle tone were also divided by the presence of HC theta accompanied by low-amplitude cortical EEG (REM sleep) or large amplitude slow activity dominating cortical and HC recordings (slow wave sleep, SWS). For analysis, multiple segments were selected from discontinuous episodes of each state dispersed over the 2 days of recordings, in which respiration appeared relatively stable without fluctuations (Table S1). Respiratory rate varied in different states in a relatively narrow band (between 1-3 Hz, Table S1) with an occasional faster component (4-6 Hz) in AW which did not overlap with theta frequency, specifically verified in each segment submitted for analysis.

EEG and EMG recordings were acquired as a ~.DDF-files in DASYLab 7.0 and then imported to Spike2 (Cambridge Electronic Devices) for signal analysis. Dia EMG recordings were processed using built-in procedures of Spike2 to remove ECG contamination and to convert high-frequency EMG components in order to retrieve pure respiratory rhythm (see details in Supplement, Fig. S2).

To quantify neuronal synchronization we used coherence analysis. Coherence function is calculated for pairs of different signals of interest (e.g., LFP recorded from two spatially distinct areas) and provides a useful measure of synchrony between two signals at each frequency of the spectrum, thus revealing characteristic frequencies of synchronization. Pairwise coherences were calculated using a program (COHER.S2S) from the Spike2 library between 5 signal pairs, representing the potential transfer of the RRO signal to higher-order structures through the OB (i.e. dia with OB and OB with PFC and HC) and between these higher order structures (i.e. PFC with HC). Power spectra for dia EMG and HC were also calculated to identify the frequencies of spectral peaks of RRO and theta rhythm. Coherence values at RRO and theta frequencies were calculated in segments selected for theta and non-theta states in urethane anesthetized rats and in SWS, REM, QW and AW in chronic experiments, recorded on two different days (Table S1). Daily averages of these values were then used in statistical analysis, including group averages (Tables 1 and S2) and comparisons of peak coherences. Differences between coherences in different states were tested using Student's t-test after Fisher r to z transformation to obtain z-scored values with normal distribution. Correlation between pair-wise coherences were statistically tested using Excel's T-DIST procedure using the formula $p=TDIST(R*SQRT((N-2)/(1-R^2)),N,1)$ where R is coherence and N is number of experiments, included.

## 3.Results

### 3.1. Respiratory rhythm in diaphragmic EMG correlates with LFP oscillations in OB

Respiratory rate varies extensively, covering in rodents the entire range of characteristic frequencies of low frequency oscillations (delta, theta, even alfa) intrinsically generated by neural circuits in the cortex and hippocampus[2]. To focus on on-going regular RROs (Fig. 1), in the present study the analysis was limited to lasting stationary segments however, excluding e.g. short segments with fast RRO potentially associated with sniffing (Fig. S3). Thus, RRO frequency was in the delta range in all states; it was below 2Hz in sleep and under urethane anesthesia and slightly faster in waking but still below theta (Table S1). Except for AW, RRO was stable in all states, manifested by a single sharp peak in the autospectra of the dia EMG signal in each recording session (Fig 2A, *left* and Fig. S4). RRO frequency in these states shifted from experiment to experiment in a narrow range, producing ~1 Hz-wide peaks in average dia autospectra (Fig. 2B). LFP in the OB correlated with this signal in a state-dependent manner (see below) giving rise to RRO peaks in the dia-OB coherence spectra, which in sleep and under urethane anesthesia were also restricted to this narrow frequency range (Fig 2C, *left*).

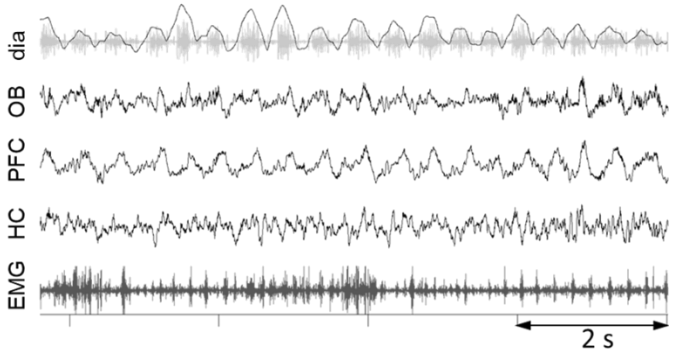


**Figure 1.** Sample of respiratory rhythm (black) derived from diaphragmal EMG (grey) along with LFPs in OB, PFC, and HC and neck muscle EMG in QW state.

In AW, RRO peaks in dia autospectra were somewhat wider in each experiment (indicating short-time scale variations within recording sessions) and its peak shifted in a wider range between experiments (1-3 Hz; Fig. 2A, *right*). In four out of 10 recordings (in 3 rats), there was a second dia power peak at 4-6 Hz, which however always appeared together with clearly distinguishable components in the 2-3 Hz range (Fig. S3C). Accordingly, group averages of dia power spectra in AW were relatively wide, with blurred maxima in the 1-3 and 5-7 Hz ranges (Fig. 2B, *right*). Dia-OB coherences were also not strictly constrained to low RRO frequencies in AW; in addition to the 1-3 Hz RRO peak there was a wide component of elevated coherences above 4 Hz in most recordings (Fig. 2E and Table S1). Therefore, in the foregoing analysis of pairwise coherences between dia, OB, PFC, and HC signals calculated at RRO peaks in individual experiments in all states was extended in AW also to coherences at the maxima in the 4.2-5.6 Hz range. This latter was verified in each recording not to coincide with HC theta frequency (Figs. 2D and S3C).

### 3.2. OB unevenly conveys RRO to higher order networks in PFC and HC

To assess RRO synchronization across regions, RRO peaks of pairwise coherences representing RRO transfer from rhythmic nasal airflow to the OB and then from OB to PFC

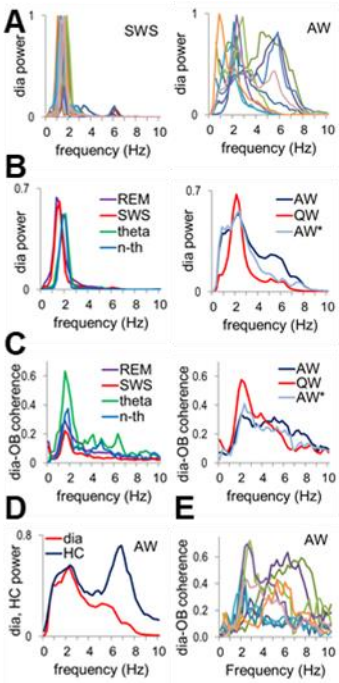


**Figure 2.** RRO oscillations in diac EMG, correlated with OB LFP. **A.** Autospectra of dia EMG in individual experiments. Note single sharp RRO peaks varying in a narrow frequency range in SWS (*left*), similar to all other states (see Fig. S3), except AW (*right*) which showed large variations and peaks at higher frequencies in a few recordings. **B**. Group averages of dia autospectra in different states. Note narrow RRO peaks in all recordings, except AW. AW*: group averages after eliminating 4 recordings with high frequency RRO. Power is shown in arbitrary units after normalization of autospectra in individual recordings setting maxima equal to 1. **C**. Group averages of dia-OB coherence spectra, in different states. Note coherence peaks constrained to RRO frequencies (dia spectral peaks) in sleep and under urethane anesthesia (*left*) and in a wider range, up to 6 Hz in QW and higher in AW (*right*). In AW, dia-OB coherence does not have a clear RRO peak on the group average due to interindividual variability of the respiratory rates (see in E). **D**. Group averages of dia and HC autospectra in AW. Note overlap of 1-3 Hz RRO in the two signals and no overlap between fast RRO in dia and theta in HC. **E**. dia-OB coherences in individual recordings.

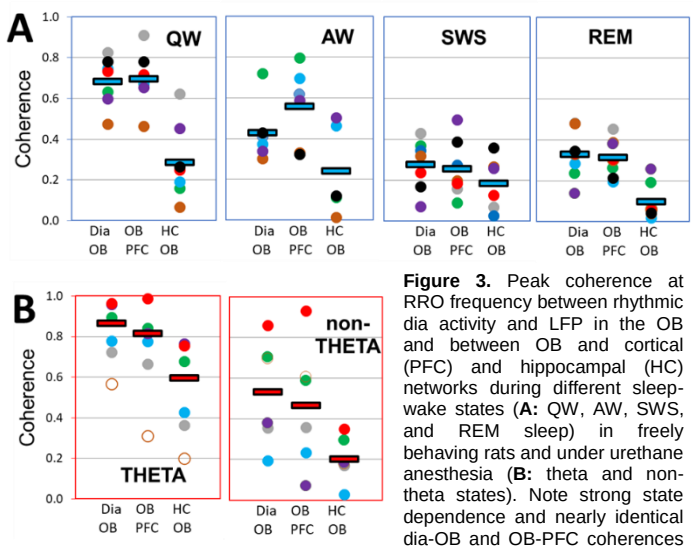


**Figure 3.** Peak coherence at RRO frequency between rhythmic dia activity and LFP in the OB and between OB and cortical (PFC) and hippocampal (HC) networks during different sleep-wake states (**A:** QW, AW, SWS, and REM sleep) in freely behaving rats and under urethane anesthesia (**B:** theta and non-theta states). Note strong state dependence and nearly identical dia-OB and OB-PFC coherences in all recordings and considerably lower OB-HC coherence both in chronic (QW, AW, REM) and anesthetized rats. Squares: group averages, dots: individual experiments; same colors identify individual rats within the chronic (n=7) and the anesthetized (n=6) groups. RRO peak coherences were found in each experiment and then averaged over the group; these averages are higher than RRO peak values of averaged coherence spectra in Figs. 4 and S5 due to slight individual variability of RRO frequency.

and HC were compared in different behavioral states. In chronic recordings, dia-OB coherences showed strong state dependence (Fig. 2C and 3A, Table 1A) and while RRO coherence between OB and PFC followed this pattern, those between OB and HC were relatively low in all states (Figs. 4, S5). Thus, OB-PFC coherences at RRO frequency were higher during wake than sleep states; differences between AW and QW vs. SWS and REMs were all statistically significant ($p<0.01$), whereas within waking and within sleep no significant differences were detected ($p>0.1$). On the other hand, group averages of OB-HC coherence fell in a narrow range; they did not change between QW, AW, and SWS and were somewhat lower in REM sleep ($p<0.1$). In all states, OB-PFC coherences were similar to dia-OB coherence (i.e. statistically equal, $p>0.1$), in major contrast to the pathway conveying RRO to HC; where OB-HC and dia-

OB coherences were significantly different in all states ($p<0.01$), except SWS. In AW, OB-PFC coherences were also higher ($p=0.09$) than OB-HC coherences in the 4.2-5.6 Hz range, as well (Fig. S6A; Table 1D).

Under urethane anesthesia (Fig. 3B, S5 and Table 1E), RRO coherences in signal-pairs of dia-OB and OB-PFC in theta state appeared closer to those in QW (although higher; $p<0.05$) than in the natural theta-dominated states of AW and REM sleep. In non-theta state they were higher than in SWS ($p=0.01$ and $p=0.03$), the presumed unanesthetized analog of this state, and were instead in the range of chronic wake states ($p>0.17$ in all comparisons). Between OB and HC, RRO coherence under urethane was higher in theta state (0.60±0.08) than in any state of chronic experiments and low in non-theta states, in the range of chronic recordings (Table 1E).

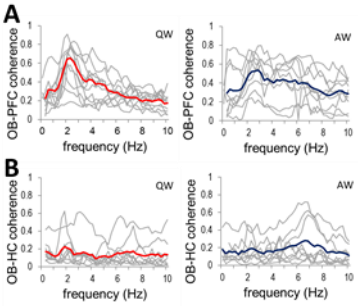


**Figure 4**. RRO coherence between OB and higher order networks of PFC and HC during waking (QW and AW). A-B. OB-PFC (A) and OB-HC (B) coherence spectra in individual experiments (grey) and averaged over the group (red and blue).

Examination of pairwise coherences in individual experiments further supported the pattern revealed by group averages; OB-HC coherence was lower than dia-OB and OB-PFC in all experiments in all states, without exception (see colors of dots, representing different experiments in Fig. 3) even though the increase in RRO coherences during wake states compared to sleep, showed natural variation between experiments. Furthermore, the variability of coherence values revealed a feature, unique for the OB-HC relationship, further separating it from dia-OB and OB-PFC. In QW and AW, as well as in theta state under urethane, the coefficient of variation (CV; Fig. 5A) indicated widely dispersed values of OB-HC coherences, compared with the other signal-pairs (CV exceeded the other two by 100-200 %; Fig. 5B).

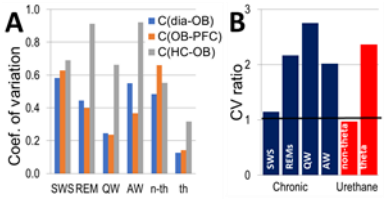


**Figure 5**. Variability of coherence values in individual experiments in different states, in freely moving (SWS, REM sleep, QW, AW) and anesthetized rats (n-th: non-theta, th: theta state). **A.** Coefficient of variation; **B**. CV ratio of coherences in the OB-HC vs. the other two signal-pairs (dia-OB and OB-PFC). Note high variation of OB-HC in waking (AW and QW), REM sleep, and urethane-theta state, 2-3 times exceeding CV of the other pairs.

To study the origin of this variability, dia-OB coherences quantifying RRO input to the OB were correlated with RRO coherences in the pathways connecting OB to the PFC and to the HC, bearing in mind that strong correlation would indicate that the more RRO is derived by OB from rhythmic nasal airflow, the more it is transferred further, to downstream targets of the OB. For the PFC this was indeed the case; we found that dia-OB and OB-PFC coherences were positively correlated (Fig 6A) in all sleep-wake states ($R>0$, $p<0.1$; Table S2), except SWS where the correlation was negative. In contrast, no such faithful, obligatory transmission of RRO through OB was found toward the HC. In chronic recordings, no significant correlation between dia-OB and OB-HC coherences was detected in waking (see grey lines in Fig. 6B), and the correlation was negative in sleep states. Thus, the consistent increase of RRO conveyed by the OB to the PFC was closely associated with RRO variation in the OB network derived from respiration (Fig. 6A), whereas RRO transmission from OB to HC, varying in a wide range from one experiment to the next (Fig. 5), did not follow the variations of dia-OB coherence in wake (AW and QW) and it was in fact showing an opposite tendency in sleep states (Fig. 6B). Similar tendency was observed in the relationship between the input and output sides of OB, i.e. positive correlation between dia-OB and OB-PFC and negative between dia-OB and OB-HC at high-frequency RRO (Fig. S6C) although the correlations were not significant (Table S2) in the low sample (n=4).

Under urethane anesthesia, both OB-PFC and OB-HC coherences showed strong correlations ($R>0$, $p<0.05$) with dia-OB coherence in both theta and non-theta states (Fig. S7, Table S2), again violating the correspondence, commonly expected on the basis of EEG signals, between urethane-theta and AW-REM on one hand and between urethane non-theta and QW-SWS on the other.

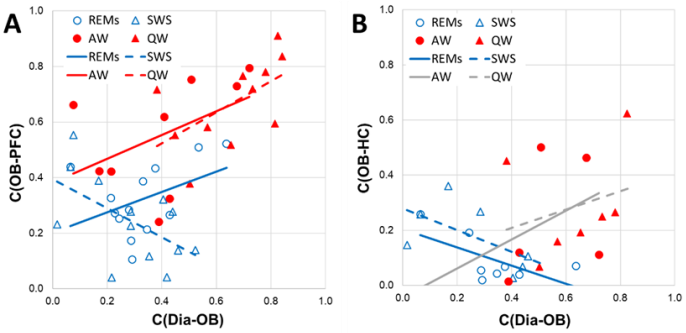


**Figure 6.** The relationship between peak RRO coherences connecting dia to OB C(Dia-OB) and those connecting OB to neural networks of PFC (**A**) and HC (**B**) in different states in chronic recordings. Trend-lines with non-significant correlations ($p>0.1$) are shown in grey,solid lines show theta, dashed line show non-theta states. Note significant positive correlation of C(dia-OB) with C(OB-PFC) but no positive correlation with C(OB-HC) in chronic experiments. C(X-Y): coherence between X and Y.

## 3.3. Role of OB-mediated RRO in coupling between higher order networks in PFC and HC

Oscillatory coupling between PFC and HC was reported in different states in freely moving rats and under Urethane anesthesia both in delta and theta frequency bands[16, 21, 22] maintained by various mono- and polysynaptic connections between the two structures. Theta peaks were dominant in PFC-HC coherence spectra during theta states (AW, REM sleep, urethane-theta) in this study, as well. Adding simultaneous dia EMG and OB recordings in this study, however, we could also identify RRO coherence peaks indicative of PFC-HC coupling at RRO frequency in the delta range. They appeared in waking animals and under urethane anesthesia, either alone (QW) or in addition to theta (AW, Urethane-theta; Fig. S8).

Average RRO coherence between PFC and HC fell in between OB-PFC and OB-HC coherence values in all states (Table 1C), although the differences were only significant in QW ($p=0.02$) with sufficient gap between OB-PFC and OB-HC coherences. PFC-HC coherence was significantly higher in waking (above 0.42) than sleep (below 0.22) and did not change

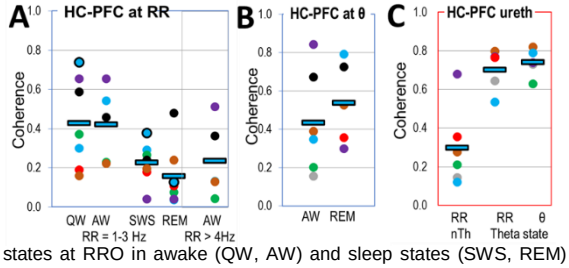


**Figure 7.** Coupling of PFC and HC networks at the RRO and theta requencies. **A**. PFC-HC coherences in different states at RRO in awake (QW, AW) and sleep states (SWS, REM) at slow (1-3 Hz) and in AW at fast RRO (>4 HZ). **B**. PFC-HC coherences at theta frequency in theta states (AW, REM). **C**. PFC-HC coherences under urethane anesthesia at RRO in non-theta and theta states and at θ in theta states. Squares: group averages, dots: individual experiments; same colors were used for individual rats in the chronic (n=7) and the anesthetized (n=6) groups (same colors as in Figs. 3 and S6).

significantly within these states (i.e. p>0.1 for AW vs. QW and REM vs. SWS comparisons) (Fig. 7A). Significant differences were also found in urethane anesthetized rats, PFC-HC RRO coherence in theta was the highest (0.7) in all states and lower in non-theta states (0.3) within the range of peak coherences in wake and sleep states (Fig. 7C; Table 1E). The relationship of OB-HC < PFC-HC < OB-PFC coherences was robust, it was also valid in most individual experiments (60 and 71% of recordings in AW and QW, 50% in urethane-theta). In theta states, coherences of the two oscillations, RRO and theta, were statistically similar in AW and urethane-theta (p>0.1), but not in REM sleep (p=0.001) (Fig. 7B,C).

Unlike theta rhythm, primarily generated in HC and conveyed to PFC[21], producing strong HC-PFC coherence, the origin of the RRO coherence between these structures is less certain. RRO is generated outside of these structures, and from the OB it is faithfully transmitted to the PFC but much less reliably to the HC (Figs. 3, 6). These differences notwithstanding, state-dependent variations in the average HC-PFC RRO coherences significantly correlated with OB-PFC ($R^2$=0.87, p=0.0003) as well as OB-HC ($R^2$=0.88, p=0.0001) coherences (Fig. 8).

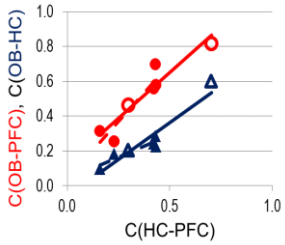


**Figure 8**. Relationship between average HC-PFC RRO coherence and RRO coherences connecting OB to PFC (red) and HC (blue) in different states in chronic recordings (AW, QW, SWS, REM; filled symbols) and under urethane anesthesia (theta and non-theta states; open symbols). Dashed lines show correlations calculated for chronic experiments only, i.e. ignoring the only high OB-HC RRO coherence in urethane anesthetized rats (OB-PFC: $R^2$=0.84, p=0.0007; OB-HC: $R^2$=0.84, p=0.0002).

RRO coherence in the PFC-HC signal-pair may be due to RRO received by PFC from OB and transmitted further to HC or may be the effect of common input from OB to PFC and HC. The first appears consistent with relatively strong, state dependent RRO in OB-PFC and HC-PFC coherences (compare Figs. 3 and 7), and the latter with the outstanding variability of RRO transmission to HC (Fig. 5) in specific states, i.e. relatively high in some experiments and lower in others in wake states and in urethane theta state (Fig. 3). To distinguish between these possible mechanisms, we next compared correlations between RRO coherences in individual experiments in each state and condition in which RRO coherences were present (Fig. 9). We investigated in particular whether stronger RRO synchrony between HC and PFC signals was associated with stronger OB-PFC or with stronger OB-HC coherences. As shown in Table 1B and Fig. 9, HC-PFC RRO coherence significantly correlated only with RRO coherences linking OB with HC but not with PFC. This relationship was found in all states showing RRO in chronic and anesthetized rats. Thus, $R^2$ correlation coefficient revealed similarity between the variations of HC-PFC and OB-HC coherences from one experiment to the next in QW ($R^2$=0.69, p=0.003), in AW at both RRO peaks ($R^2$=0.79, p=0.01 for slow and $R^2$=0.68, p=0.026 for fast RRO; Table 1B and 1D), and in urethane-theta state ($R^2$=0.72, p=0.02; Table 1E).

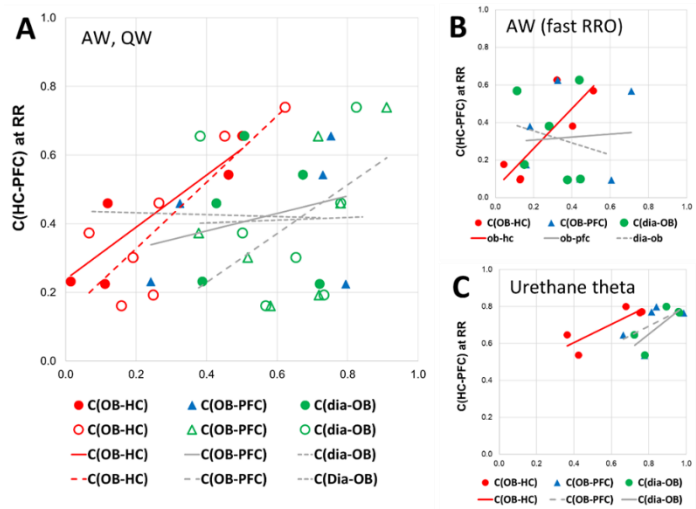


**Figure 9.** Correlation between peak RRO coherences C(HC-PFC) connecting PFC and HC vs. RRO coherences connecting OB to dia, PFC, and HC signals (C(dia-OB), C(OB-PFC), C(OB-HC), respectively) in AW and QW in chronic recordings at low (**A**) and high frequency RRO (**B**) and in theta state under urethane anesthesia (**C**). Significant correlations are shown in the color of the corresponding dots, trendlines of non-significant correlations are shown in grey.

In contrast, HC-PFC coherence did not correlate with OB-PFC coherence in any state (Table 1B, 1D, and 1E). Positive trends were observed in QW ($R^2$=0.33) and urethane-theta ($R^2$=0.30) states but were not significant (p=0.06 and p=0.16, respectively; see grey lines in Fig. 9). Variations of HC-PFC coherence in individual experiments was not affected by variations of dia-OB coherence in waking states and by any coherence connecting dia, OB, PFC, HC signals during sleep (Fig. S9).

**Table 1.** Relationship between coherences through OB and their effect on RRO synchronization between PFC and HC. Yellow background highlights relatively high coherences, above 0.4 and significant correlations (p < 0.05), $R^2$, between pairwise coherences. C(X-Y): coherence between X and Y.

**A.** Coherences connecting OB to dia and LFP signals of PFC and HC, at RRO frequency

| Peak Coherence | SWS | REM | QW | AW |
|---|---|---|---|---|
| C(Dia-OB) | 0.29±0.04 | 0.33±0.04 | 0.66±0.05 | 0.40±0.07 |
| C(OB-PFC) | 0.25±0.04 | 0.32±0.04 | 0.67±0.05 | 0.55±0.07 |
| C(OB-HC) | 0.18±0.05 | 0.09±0.03 | 0.29±0.07 | 0.24±0.10 |

**B**. Correlations between C(HC-PFC) and coherences connecting OB to other signals

| $R^2$ between C(PFC-HC) and… | SWS | REM | QW | AW |
|---|---|---|---|---|
| … C(Dia-OB) | 0.08 | 0.01 | 0.00 | 0.00 |
| … C(OB-PFC) | 0.04 | 0.07 | 0.33 | 0.12 |
| … C(OB-HC) | 0.27 | 0.00 | 0.69 | 0.79 |

**C.** Coherences connecting LFP signals of PFC and HC, at RRO frequency

| peak coherence | SWS | REM | QW | AW |
|---|---|---|---|---|
| C(PFC-HC) | 0.22±0.04 | 0.19±0.07 | 0.45±0.08 | 0.42±0.09 |

**D**. At high frequency RRO in AW

| Coherence | AW |
|---|---|
| C(Dia-OB) | 0.34±0.05 |
| C(OB-PFC) | 0.46±0.06 |
| C(OB-HC) | 0.26±0.07 |
| C(PFC-HC | 0.32±0.10 |

| $R^2$ between C(PFC-HC) and… | AW |
|---|---|
| … C(Dia-OB) | 0.04 |
| … C(OB-PFC) | 0.01 |
| … C(OB-HC) | 0.68 |

**E**. Under urethane anesthesia

| Coherence | Urethane | |
|---|---|---|
| | Non-theta | Theta |
| C(Dia-OB) | 0.53±0.11 | 0.87±0.06 |
| C(OB-PFC) | 0.47±0.13 | 0.82±0.09 |
| C(OB-HC) | 0.20±0.05 | 0.60±0.08 |
| C(PFC-HC) | 0.30±0.08 | 0.70±0.05 |

| $R^2$ between C(PFC-HC) and… | Urethane | |
|---|---|---|
| | Non-theta | Theta |
| … C(Dia-OB) | 0.87 | 0.63 |
| … C(OB-PFC) | 0.92 | 0.30 |
| … C(OB-HC) | 0.88 | 0.72 |

## 4. Discussion

This study used inter-regional coherences and their correlations to trace the RRO signal from OB, where it is derived from rhythmic nasal airflow, to higher order brain networks of PFC and HC where it may potentially contribute to communication between these structures by synchronizing their activities at the respiratory rate. We focused in particular on on-going, i.e. "background", RRO unaffected by behaviors requiring its short-term fluctuations, e.g. sniffing. We found that this rhythmicity depends on sleep-wake states; it is significantly larger in waking than in sleep whereas within these arousal states remains unchanged when the animal is engaged in behaviors or conditions associated with theta or non-theta HC activity, i.e. in exploration, locomotion (AW), and REM sleep vs. consummatory behaviors (QW) and SWS. In agreement with previous reports[3, 4, 9, 24], RRO was more prominent in PFC with an obligatory transmission of RRO from OB to PFC, indicated by parallel variations in dia-OB and OB-PFC coherences in individual experiments, verified by significant correlation between these parameters over the group. In contrast, RRO was relatively low in HC and the variations of OB-HC coherence did not necessarily follow those between dia and OB. RRO input to HC[5-7] however lead to strong variations in individual recordings not explained by the grossly defined states of AW and QW. Importantly, this factor, quantified with OB-HC coherence, was essential for establishing PFC-HC synchrony at the respiratory rate, whereas variations of RRO in OB and PFC had no significant effect. Furthermore, we found that RRO under urethane had no resemblance with sleep; the two states identified in urethane-anesthetized rats were more similar to wake states in freely behaving rats.

**4.1. RRO in waking.** Communication and collaboration between HC and PFC and its impairment in psychiatric diseases has been the primary focus of extensive research to date[18-21]. HC theta driven PFC synchronization and its role in spatial working memory is relatively well-studied[25-30]. On the other hand, PFC is theorized to be the master regulator of working memory and higher-order executive function[31-36], yet the mechanisms by which PFC exerts "top-down" influences remain less clear. Functional coupling of PFC with downstream circuits, including HC, amygdala, ventral tegmental area, by means of delta-range oscillations (2-5 Hz) was recently shown in PFC-specific tasks[14-16] and it was proposed that theta and delta oscillations may serve as parallel channels of communication in opposite directions between the HC and the PFC[22]. The results of the present study indicate that the balance and interaction between theta and RRO may also provide a potential mechanism for bidirectional HC-PFC coupling. When RRO is within the delta range, it can contribute to or even drive the PFC 2-5 Hz rhythm[37, 38]. PFC receives this input whenever OB detects RRO and may broadcast it widely. In contrast, the connection of HC to this global[2] rhythm appears more dynamic; in episodes when HC becomes receptive to RRO input this could open a PFC-to-HC channel in the delta range distinct from the channel established by HC-theta in the opposite direction.

The most striking observation of this study was the marked contrast between the strength and reliability of RRO input, i.e. stronger in PFC than in HC (Table 1A), and its effect on PFC-HC coherence, i.e. HC stronger than PFC (Table 1B), raising questions regarding the mechanisms and the functional consequences. Differences in cytoarchitecture, connectivity, and other characteristics of PFC and HC networks give rise to different intrinsic oscillations in the two structures allowing them to resonate with rhythmic input at specific frequencies. We propose that due to these differences, baseline slow RRO recorded in this study may be involved in PFC-HC communication primarily in the of PFC-to-HC direction.

Task-related intrinsic oscillations in PFC appear at frequencies in the delta range[14-16]. Notably, these oscillations in waking are markedly different from the wide-band thalamo-cortical delta rhythm of SWS; their spectra are narrow-band, they are hierarchically nested with gamma oscillations[39, 40], and are normally generated in cortico-cortical circuits, associated with various cognitive functions[40-43]. Outgoing PFC messages aligned with these oscillations may use the fluctuations in sensitivity of downstream structures tuned to global RRO, when the two are synchronized. This may include HC, when RRO is present outside of sniffing[5-7] making it sensitive to messages arriving assembled in bouts at delta-range frequencies.

On the other hand, background RRO is slower than HC theta rhythm and thus, in order to synchronize with the signature HC oscillation during active states of sniffing, respiratory rate is accelerated and brought within the higher and narrower theta frequency band. The two oscillations, RRO and theta, show distinct characteristics in HC, such as different laminar profiles and theta-modulated gamma bands, and differentially entrained HC neurons[5-7] even when their frequencies overlap. However, during these episodes, olfactory-related activity patterns in OB, such as cell firing and gamma bursts, appear phase locked to the RRO-theta rhythm[44]. The exact mechanisms are not completely understood, but rhythmic synchronization of sensory sampling in OB on one hand and excitability of neurons involved in central processing in HC and piriform cortex on the other is considered a "paradigmatic example" of active sensing[11, 45] optimizing odor perception coordinated with multiple sensory channels, in turn associated with rhythmic nasal, whisker, and head movements.

Although lacking strong direct projections from the OB[6, 46, 47], both structures receive RRO via multisynaptic pathways which includes common connections, e.g. through piriform cortex, as well as uneven projections, e.g. through amygdala (PFC) or entorhinal cortex (HC)[3, 6], and thus PFC-HC coherence may emerge from common OB input. Alternatively, or in addition, strong RRO may be directed primarily to PFC and then transmitted further to HC. Nodes in centripetal OB projections and in pathways connecting PFC and HC (see e.g.[22, 48]) may set the balance of RRO between the two structures.

When and how HC couples with slow baseline RRO will require further investigations using specific tasks beyond gross sleep-wake states pursued in this study. Data demonstrating the potential role of RRO in non-olfactory processing started to accumulate in recent years not only from rodent but human studies as well[10, 49, 50]. A specific challenge for translating the results between species is due to important differences between human and rodents. Brain oscillations, their function, dynamics,

and key features including their characteristic frequencies, are evolutionarily well-preserved[51], but respiratory rate varies widely between species. In human, where respiratory rate (~0.2 Hz) is below the frequencies of the key components of the EEG oscillatory hierarchy, RRO is manifested by phase-amplitude modulation of oscillations rather than coherence in different frequency bands, including slow (delta, theta) as well as fast (beta, gamma) oscillations, involved in cognitive processes[10]. This is a different form of coupling which unlike coherence does not require matching the frequencies of rhythms generated by different mechanisms.

**4.2. RRO in sleep.** In contrast to wake states, RRO during sleep appears reduced already at the level of OB indicated by relatively low dia-OB coherence (Fig. 3) thus restricting OB-mediated RRO in higher brain structures (PFC, HC) from coupling with oscillations dominant in these networks during sleep. Viczko et al.[52] demonstrated for example that slow oscillations (SO), an archetypical EEG pattern in SWS, emerges separate from respiration even when they overlap in frequency and argued that it "fit with an SO mechanism as intrinsic emergent property of a deafferented neural network". Our data is in-line with this concept, suggesting that intrinsic brain oscillations, relevant in sleep-dependent memory consolidation both in SWS (SO[52] and delta[53]) and REM sleep (theta[54]), are protected from RRO. It is interesting to note that in human, where very few studies analyzed RRO during sleep with statistical scrutiny[55, 56], subtle changes in EEG linked to respiratory cycles were enhanced in SWS and REM sleep in children with sleep disordered breathing in multiple frequency bands, including delta[55], theta[55, 56], alpha, and sigma[56]. Adenotonsillectomy, the most common surgical procedure for sleep apnea which among other benefits improves cognitive function, reduced i.e. normalized these RRO alterations.

It is important to note however that our conclusions only concern rhythmic RRO mediated by the OB. It has been reported that, besides RRO, respiration may also pace non-rhythmic events, linking their occurrence to specific phases of respiration (see e.g.[13, 49]). In sleep, this may include sharp wave/ripples and dentate spikes, i.e. intrinsic HC patterns during SWS synchronized with UP-DOWN transitions in cortical networks that are involved in functional PFC-HC interactions serving memory consolidation[57, 58]. In a recent study, Karalis and Sirota[59] found that the post-inspiratory bias of these patterns along with firing of a large number of PFC and HC neurons remained after deafferentation of OB sensory neurons, indicating that mechanisms bypassing the OB play a primary role in their synchronization. They hypothesized the contribution of a "so-far undescribed ascending respiratory corollary discharge signal, likely propagating from the brainstem respiratory rhythm generators" which could pace limbic networks using a disinhibition-mediated mechanism, consistent with lack of prominent LFPs in the absence of input from the OB[59]. The causal model remains to be elucidated, however. Besides ascending projections from the preBötzinger complex[60] or the locus coeruleus[61], a number of other signals from internal organs due to respiratory movements and chemosensitive signals from the cardiovascular system may be involved[13, 62, 63].

**4.3. RRO under urethane anesthesia.** We found major differences between RRO in sleep and under urethane anesthesia which raise important questions about the traditional use of the latter for modeling oscillatory networks in sleep[7, 52, 64]. It is known that different types of brain oscillations better survive urethane anesthesia[65-68], compared with many other anesthetics. It is especially compelling that HC theta rhythm appears spontaneously in this preparation, alternating with non-theta states, and can also be elicited by brainstem stimulation thus offering a viable model for mechanistic investigations of generating this rhythm and related neuropharmacology[69-71]. The major strength of the model is that behavioral confounds of waking (e.g. locomotion, cognition) on one hand and fragmentation of sleep patterns (e.g. REM sleep never lasts longer than a few minutes in rodents) on the other are effectively eliminated. But this comes with the price of uncertainties in the interpretation of alternating theta and non-theta states as changes between QW and AW or between SWS and REM sleep brain-states. RRO mechanisms were also explored under urethane anesthesia[6, 7, 52] interpreting the results mostly in terms of modeling active and passive sleep states. Indeed, stable respiratory rate, along with several other parameters (e.g. genioglossus muscle atonia[72]) in theta state resembles REM sleep more than AW. The results of this study however suggest a cautious approach when interpreting the results of RRO under urethane anesthesia. RRO coherences in urethane anesthetized rats were higher than in SWS and REM sleep and in urethane theta state were even higher than in AW and QW. Under urethane anesthesia RRO transmission through OB showed marked differences between active and passive states, unlike in chronic AW vs. QW comparisons. The pattern of pairwise RRO coherences connecting OB with the three other signals detected in waking was similar to that in urethane non-theta and the pattern of their correlation with PFC-HC coherence in theta states. These differences should be carefully considered in mechanistic studies of RRO mechanisms in the urethane model, in the future.

## Supplemental Information

**Perfusion and Histology.** Perfusion was conducted by inserting a hypodermic needle connected to a pump into the ascending aorta through the left ventricle of the heart. The right ventricle was cut open and phosphate buffered saline (PBS) was pumped into the circulation system for 5 minutes, until all blood had been drained and replaced with PBS. Then 10% buffered formalin solution was pumped for about 15-20 minutes, until the rat was stiff. After perfusion, the rats' brain was carefully extracted and placed in a vial filled with 20 mL of formalin for further fixation for at least one hour, while stored at 4ºC. Before cryosectioning (Microm, HM 450), the brains were stored in 20% sucrose solution overnight at 4 °C until sank to the bottom of the vial. 45 µm slices were stored in PBS with Azide and then mounted on slides and

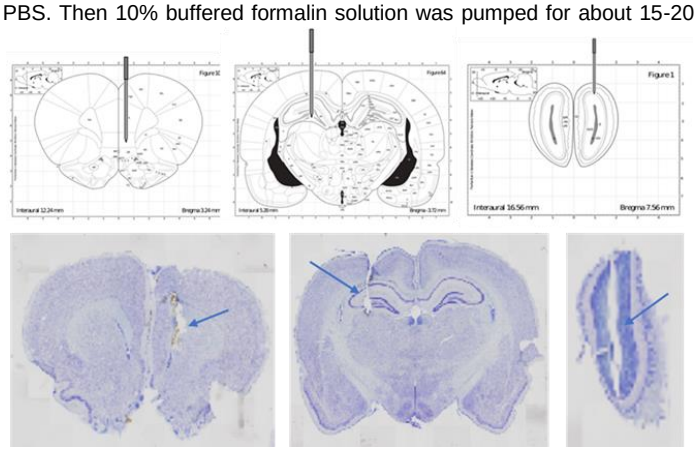

**Figure S1.** Placement of electrodes for local field potential (LFP) recordings. Schematic drawing (*top*) and histology of stained coronal sections (*bottom*) to identify electrode coordinates in the prefrontal cortex (PFC), hippocampus (HC), and olfactory bulb (OB).

stained with Cresyl Violet, coverslipped and evaluated to locate the marks of damage due to inserted recording electrodes (Fig. S1).

**Measurements of respiration.** There are various methods for recording respiration in rodents. The most well-known and commonly used are whole-body plethysmography and measuring nasal airflow using thermocouples or thermistors. Plethysmograph is an apparatus designed for reliably measuring the variations of the body volume during ventilation. This method however requires confining the animal to a small chamber which represents serious limitations for behavior, and thus was unacceptable for our paradigm of recording EEG during normal undisturbed behaviors in freely moving rats[73]. Thermocouples and thermistors are small devices that contain sensors to measure the changes in the temperature of the airflow, in the nose or the mouth. During inspiration, the airflow has the same temperature as air in the room whereas, during expiration, the temperature would follow the body temperature[74]. These are simple devices which are relatively easy to use but have to be implanted through invasive procedures, which may contribute to changes in the natural behavior of the animal[73]. Additionally, previous studies showed that thermocouple recording of respiration is unreliable during sleep and specifically during REM sleep. This can be explained by the reduced volume of the airflow during sleep, which may provide inaccurate data.

In this project we developed an alternative method for the monitoring respiration by measuring the muscle activity of the diaphragm. According to our experience, this allows reliable monitoring of breathing in different states, including REM-sleep, without the difficulties and errors of the other measurements mentioned above. It's an invasive and quick surgical method, taking around 30 minutes, performed at the time of surgical implantation of the EEG electrodes; there were no signs of changing the normal behavior of the rats. A well-performed surgery developed in this project is also suitable for different experiments including behaviors in cognitive tasks e.g. during freezing or tasks using a T-maze. The electrodes are chronic and could be left inside the animals until the time of euthanasia. This method showed good results in almost all rats in this project for up to 3 weeks after the surgery. None of the rats showed any signs of infections or rejections of the implant.

Diaphragmal EMG recordings were processed using built-in procedures of Spike2 to remove ECG contamination and convert high-frequency EMG components to retrieve pure respiratory rhythm (Fig. S2). First, the recording was high-pass filtered above 350-400 Hz which gave the signal an "EMG shape" by eliminating slow fluctuations. Next, the half-wave rectified signal was passed to a Spike2 algorithm to generate a new "virtual channel" to cut off all EKG-related noises above a certain voltage level identified individually in different experiments. The final respiratory signal was then generated using Spike2 "RMS amplitude" and "smooth" procedures.

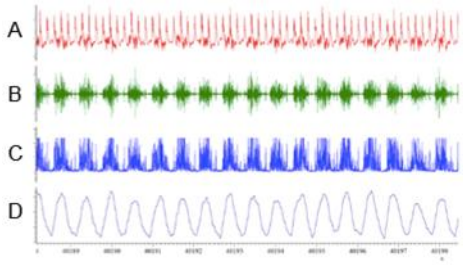


**Figure S2.** Processing of dia EMG. Ten second sample raw signal with high ECG contamination (A), high-pass filtered above 350 - 400 Hz (B), rectified (C), and smoothed to derive RMS-amplitude

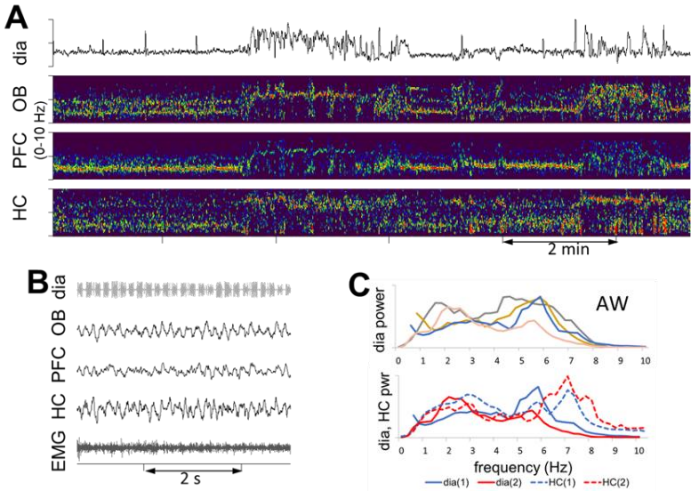


**Figure S3.** Unstable RRO in AW. Example of segments with RRO matching theta frequency, presumably associated with sniffing and excluded from analysis in this study (A-B) and segments with slow and faster RRO not synchronized with theta frequency (C). **A**. Rapidly alternating episodes of slow and fast respiration, presumably associated with sniffing. Respiration and time-frequency plots of LFP signals are shown in the 0-10 Hz range. Note matching frequencies of different signals in slow RRO and theta segments. **B**. Example of theta segment with RRO at theta frequency. **C.** *Top:* Two spectral peaks in dia autospectra, one at 2-3 Hz, the other at 4-6 Hz, in 4 out of 10 AW recordings. *Bottom:* Dia (solid lines) and HC (dashed lines) autospectra showing that high RRO did not overlap with HC theta.

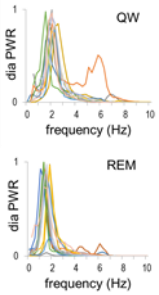


**Figure S4.** Autospectra of diaphragmal EMG in individual experiments in QW and REM sleep.

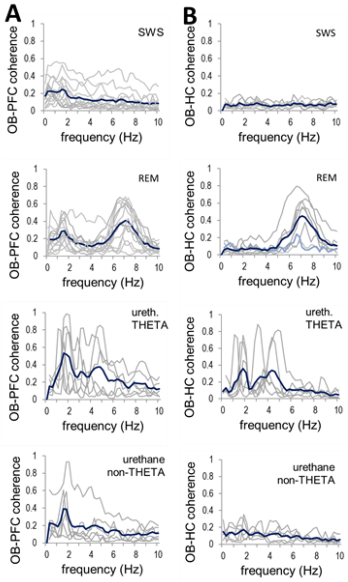


**Figure S5.** RRO coherence between OB and higher order networks of PFC and HC in sleep (SWS, REM) and under urethane anesthesia (theta and non-theta states). A-B. OB-PFC (A) and OB-HC (B) coherence spectra in individual experiments (grey) and averaged over the group (red).

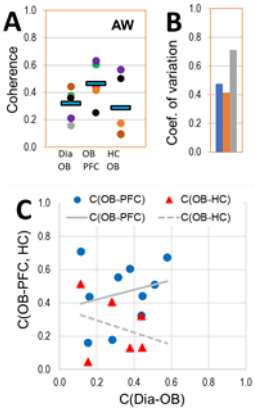


**Figure S6.** Coherences between dia, OB, PFC, and HC in AW at the high-frequency component of RRO (4.2-5.6 Hz). **A**. Peak coherences in individual experiments (dots) and group averages (squares). **B**. Coefficient of Variation (CV) of C(dia-OB), C(OB-PFC) and, and C(OB-HC) coherences. **C**. No significant correlation between coherences representing respiratory input to OB, i.e. C(dia-OB), and RRO at the OB output (C(OB-PFC): R=0.24, p=0.25, n=10; C(OB-HC): R=-0.29, p=0.31, n=6). (CF A, B, and C with Figs. 3, 5, and 6, respectively)

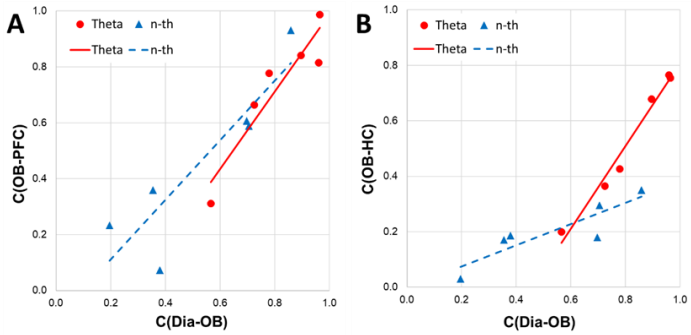


**Figure S7.** The relationship between peak RRO coherences connecting dia to OB and those connecting OB to PFC (**A**) and HC networks (**B**) under urethane anesthesia. Note significant positive correlation of C(dia-OB) with C(OB-PFC) and C(OB-HC) under anesthesia (theta and non-theta). C(X-Y): coherence between X and Y.

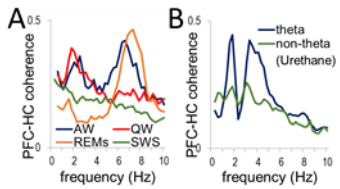


**Figure S8.** Oscillatory coupling between higher order networks of PFC and HC. PFC-HC coherences during different states in chronic recordings (**A**) and under urethane anesthesia (**B**). Note peaks at RRO (~2 Hz in chronic and 1-2 Hz under urethane) and at theta frequencies (6-8 Hz in chronic and 3-5 Hz under Urethane), in specific states.

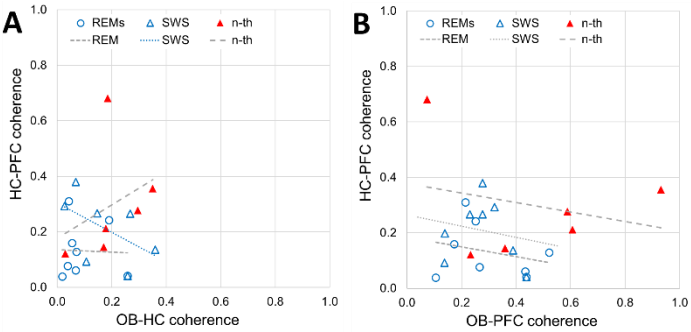


**Figure S9.** Correlation between peak RRO coherences between PFC and HC, and RRO coherences connecting OB to PFC (**A**), and HC signals (**B**) in different conditions and states with weak or non-existent RRO (REM sleep, SWS, urethane non-theta state). Significant correlations are shown in the color of the corresponding dots, trendlines of non-significant correlations are shown in grey.

**Table S1:** length of segments and average RRO and theta frequency in different states

| | SWS | REM | QW | AW | Urethane Theta | Urethane Non-theta |
|---|---|---|---|---|---|---|
| in each rat (2 days):<br># of segments<br>Ave length (s)<br>Total length (s) | 9±0.8<br>127±11<br>1237 ±219 | 9±0.9<br>109±12<br>1031 ±186 | 7±0.4<br>112±18<br>821 ±147 | 7±0.5<br>95±14<br>670 ±98 | 6±0.8<br>135±40<br>825 ±276 | 5±0.7<br>96±20<br>471 ±95 |
| # of rats (recordings) with identified RRO in LFP | 7(14) | 7(14) | 7(12) | 6(9)<br>Fast RRO: 6(10) | 5(5) | 6(6) |
| RRO peak frequency (Hz) and range (Hz) | 1.65 ±0.05 1.2-2.0 | 1.65 ±0.05 1.2-2.0 | 2.01 ±0.08 1.5-2.4 | 2.23 ±0.11 1.0-2.9<br>4.86 ±0.18 4.2-5.6 | 1.80 ±0.14 1.2-2.2 | 1.73 ±0.14 1.2-2.0 |
| Theta freq. (Hz) and range (Hz) | | 7.08±0.09 6.8-7.3 | | 6.84 ±0.13 6.6-7.1 | 3.95 ±0.26 3.2-4.9 | |

**Table S2:** Correlation between dia-OB coherences and OB-PFC and OB-HC (significant positive correlation is marked with colored background, yellow: p<0.05, orange: 0.05<p<0.1). C(X-Y): coherence between X and Y.

| R2 between C(dia-OB) and… | SWS | REM | QW | AW | Urethane Theta | Urethane Non-theta |
|---|---|---|---|---|---|---|
| … C(OB-PFC) | 0.31 (-) | 0.17 | 0.33 | 0.21<br>0.06 | 0.87 | 0.80 |
| … C(OB-HC) | 0.35 (-) | 0.41 (-) | 0.08 | 0.12<br>0.08 | 0.99 | 0.78 |

## References


1. Adrian, E.D. Olfactory reactions in the brain of the hedgehog. *J Physiol* **100**, 459-473 (1942).
2. Tort, A.B.L., Brankack, J. & Draguhn, A. Respiration-Entrained Brain Rhythms Are Global but Often Overlooked. *Trends Neurosci* **41**, 186-197 (2018).
3. Biskamp, J., Bartos, M. & Sauer, J.F. Organization of prefrontal network activity by respiration-related oscillations. *Sci Rep* **7**, 45508 (2017).
4. Zhong, W., *et al.* Selective entrainment of gamma subbands by different slow network oscillations. *Proc Natl Acad Sci U S A* **114**, 4519-4524 (2017).
5. Nguyen Chi, V., *et al.* Hippocampal Respiration-Driven Rhythm Distinct from Theta Oscillations in Awake Mice. *J Neurosci* **36**, 162-177 (2016).
6. Yanovsky, Y., Ciatipis, M., Draguhn, A., Tort, A.B. & Brankack, J. Slow oscillations in the mouse hippocampus entrained by nasal respiration. *J Neurosci* **34**, 5949-5964 (2014).
7. Lockmann, A.L., Laplagne, D.A., Leao, R.N. & Tort, A.B. A Respiration-Coupled Rhythm in the Rat Hippocampus Independent of Theta and Slow Oscillations. *J Neurosci* **36**, 5338-5352 (2016).
8. Ito, J., *et al.* Whisker barrel cortex delta oscillations and gamma power in the awake mouse are linked to respiration. *Nat Commun* **5**, 3572 (2014).
9. Tort, A.B.L., *et al.* Parallel detection of theta and respiration-coupled oscillations throughout the mouse brain. *Sci Rep* **8**, 6432 (2018).
10. Zelano, C., *et al.* Nasal Respiration Entrains Human Limbic Oscillations and Modulates Cognitive Function. *J Neurosci* **36**, 12448-12467 (2016).
11. Corcoran, A.W., Pezzulo, G. & Hohwy, J. Commentary: Respiration-Entrained Brain Rhythms Are Global but Often Overlooked. *Front Syst Neurosci* **12**, 25 (2018).
12. Heck, D.H., Kozma, R. & Kay, L.M. The rhythm of memory: how breathing shapes memory function. *J Neurophysiol* **122**, 563-571 (2019).
13. Heck, D.H., *et al.* Breathing as a Fundamental Rhythm of Brain Function. *Front Neural Circuits* **10**, 115 (2016).
14. Dejean, C., *et al.* Prefrontal neuronal assemblies temporally control fear behaviour. *Nature* **535**, 420-424 (2016).
15. Karalis, N., *et al.* 4-Hz oscillations synchronize prefrontal-amygdala circuits during fear behavior. *Nat Neurosci* **19**, 605-612 (2016).
16. Fujisawa, S. & Buzsaki, G. A 4 Hz oscillation adaptively synchronizes prefrontal, VTA, and hippocampal activities. *Neuron* **72**, 153-165 (2011).
17. Buzsaki, G. Theta oscillations in the hippocampus. *Neuron* **33**, 325-340 (2002).
18. Sigurdsson, T., Stark, K.L., Karayiorgou, M., Gogos, J.A. & Gordon, J.A. Impaired hippocampal-prefrontal synchrony in a genetic mouse model of schizophrenia. *Nature* **464**, 763-767 (2010).
19. Lee, H., *et al.* Early cognitive experience prevents adult deficits in a neurodevelopmental schizophrenia model. *Neuron* **75**, 714-724 (2012).
20. Dickerson, D.D., Wolff, A.R. & Bilkey, D.K. Abnormal long-range neural synchrony in a maternal immune activation animal model of schizophrenia. *J Neurosci* **30**, 12424-12431 (2010).

21. Nandi, B., Swiatek, P., Kocsis, B. & Ding, M. Inferring the direction of rhythmic neural transmission via inter-regional phase-amplitude coupling (ir-PAC). *Sci Rep* **9**, 6933 (2019).

22. Roy, A., Svensson, F.P., Mazeh, A. & Kocsis, B. Prefrontal-hippocampal coupling by theta rhythm and by 2-5 Hz oscillation in the delta band: The role of the nucleus reuniens of the thalamus. *Brain Struct Funct* **222**, 2819-2830 (2017).

23. Paxinos, G. & Watson, C. *The Rat Brain in Stereotaxic Coordinates.* (Academic Press, Sydney, 1986).

24. Heck, D.H., *et al.* Cortical rhythms are modulated by respiration. *BioRxiv*, 049007 (2016).

25. Sarnthein, J., Petsche, H., Rappelsberger, P., Shaw, G.L. & von Stein, A. Synchronization between prefrontal and posterior association cortex during human working memory. *Proc Natl Acad Sci U S A* **95**, 7092-7096 (1998).

26. Igarashi, K.M. Plasticity in oscillatory coupling between hippocampus and cortex. *Curr Opin Neurobiol* **35**, 163-168 (2015).

27. Zhang, X., *et al.* Impaired theta-gamma coupling in APP-deficient mice. *Sci Rep* **6**, 21948 (2016).

28. Kaplan, R., *et al.* Medial Prefrontal-Medial Temporal Theta Phase Coupling in Dynamic Spatial Imagery. *J Cogn Neurosci* **29**, 507-519 (2017).

29. Tamura, M., Spellman, T.J., Rosen, A.M., Gogos, J.A. & Gordon, J.A. Hippocampal-prefrontal theta-gamma coupling during performance of a spatial working memory task. *Nat Commun* **8**, 2182 (2017).

30. Barr, M.S., *et al.* Impaired theta-gamma coupling during working memory performance in schizophrenia. *Schizophr Res* **189**, 104-110 (2017).

31. Teffer, K. & Semendeferi, K. Human prefrontal cortex: evolution, development, and pathology. *Prog Brain Res* **195**, 191-218 (2012).

32. Fletcher, P.C., Shallice, T., Frith, C.D., Frackowiak, R.S. & Dolan, R.J. The functional roles of prefrontal cortex in episodic memory. II. Retrieval. *Brain* **121 ( Pt 7)**, 1249-1256 (1998).

33. Fletcher, P.C., Shallice, T. & Dolan, R.J. The functional roles of prefrontal cortex in episodic memory. I. Encoding. *Brain* **121 ( Pt 7)**, 1239-1248 (1998).

34. Buckner, R.L. & Wheeler, M.E. The cognitive neuroscience of remembering. *Nat Rev Neurosci* **2**, 624-634 (2001).

35. Miller, E.K. & Cohen, J.D. An integrative theory of prefrontal cortex function. *Annu Rev Neurosci* **24**, 167-202 (2001).

36. Benchenane, K., Tiesinga, P.H. & Battaglia, F.P. Oscillations in the prefrontal cortex: a gateway to memory and attention. *Curr Opin Neurobiol* **21**, 475-485 (2011).

37. Kocsis, B., Pittman-Polletta, B.R. & Roy, A. Respiration-coupled rhythms in prefrontal cortex: beyond if, to when, how, and why. *Brain Struct Funct* **223**, 11-16 (2018).

38. Lockmann, A.L.V. & Tort, A.B.L. Nasal respiration entrains delta-frequency oscillations in the prefrontal cortex and hippocampus of rodents. *Brain Struct Funct* **223**, 1-3 (2018).

39. Pittman-Polletta, B., Hu, K. & Kocsis, B. Subunit-specific NMDAR antagonism dissociates schizophrenia subtype-relevant oscillopathies associated with frontal hypofunction and hippocampal hyperfunction. *Sci Rep* **8**, 11588 (2018).

40. Hunt, M.J., Kopell, N.J., Traub, R.D. & Whittington, M.A. Aberrant Network Activity in Schizophrenia. *Trends Neurosci* **40**, 371-382 (2017).

41. Hall, T.M., de Carvalho, F. & Jackson, A. A common structure underlies low-frequency cortical dynamics in movement, sleep, and sedation. *Neuron* **83**, 1185-1199 (2014).

42. Nacher, V., Ledberg, A., Deco, G. & Romo, R. Coherent delta-band oscillations between cortical areas correlate with decision making. *Proc Natl Acad Sci U S A* **110**, 15085-15090 (2013).

43. Riecke, L., Sack, A.T. & Schroeder, C.E. Endogenous Delta/Theta Sound-Brain Phase Entrainment Accelerates the Buildup of Auditory Streaming. *Curr Biol* **25**, 3196-3201 (2015).

44. Kay, L.M., *et al.* Olfactory oscillations: the what, how and what for. *Trends Neurosci* **32**, 207-214 (2009).

45. Wachowiak, M. All in a sniff: olfaction as a model for active sensing. *Neuron* **71**, 962-973 (2011).

46. Hoover, W.B. & Vertes, R.P. Anatomical analysis of afferent projections to the medial prefrontal cortex in the rat. *Brain Struct Funct* **212**, 149-179 (2007).

47. Moberly, A.H., *et al.* Olfactory inputs modulate respiration-related rhythmic activity in the prefrontal cortex and freezing behavior. *Nat Commun* **9**, 1528 (2018).

48. Bagur, S. & Benchenane, K. Taming the oscillatory zoo in the hippocampus and neo-cortex: a review of the commentary of Lockmann and Tort on Roy et al. *Brain Struct Funct* **223**, 5-9 (2018).

49. Perl, O., *et al.* Human non-olfactory cognition phase-locked with inhalation. *Nat Hum Behav* **3**, 501-512 (2019).

50. Arshamian, A., Iravani, B., Majid, A. & Lundstrom, J.N. Respiration Modulates Olfactory Memory Consolidation in Humans. *J Neurosci* **38**, 10286-10294 (2018).

51. Buzsaki, G. & Draguhn, A. Neuronal oscillations in cortical networks. *Science* **304**, 1926-1929 (2004).

52. Viczko, J., Sharma, A.V., Pagliardini, S., Wolansky, T. & Dickson, C.T. Lack of respiratory coupling with neocortical and hippocampal slow oscillations. *J Neurosci* **34**, 3937-3946 (2014).

53. Kim, J., Gulati, T. & Ganguly, K. Competing Roles of Slow Oscillations and Delta Waves in Memory Consolidation versus Forgetting. *Cell* **179**, 514-526 e513 (2019).

54. Boyce, R., Glasgow, S.D., Williams, S. & Adamantidis, A. Causal evidence for the role of REM sleep theta rhythm in contextual memory consolidation. *Science* **352**, 812-816 (2016).

55. Chervin, R.D., *et al.* Correlates of respiratory cycle-related EEG changes in children with sleep-disordered breathing. *Sleep* **27**, 116-121 (2004).

56. Immanuel, S.A., *et al.* Respiratory cycle-related electroencephalographic changes during sleep in healthy children and in children with sleep disordered breathing. *Sleep* **37**, 1353-1361 (2014).

57. Sirota, A. & Buzsaki, G. Interaction between neocortical and hippocampal networks via slow oscillations. *Thalamus Relat Syst* **3**, 245-259 (2005).

58. Sirota, A., Csicsvari, J., Buhl, D. & Buzsaki, G. Communication between neocortex and hippocampus during sleep in rodents. *Proc Natl Acad Sci U S A* **100**, 2065-2069 (2003).

59. Karalis, N. & Sirota, A.M. Breathing coordinates limbic network dynamics underlying memory consolidation. *BioRxiv* (2018).

60. Yang, C.F. & Feldman, J.L. Efferent projections of excitatory and inhibitory preBotzinger Complex neurons. *J Comp Neurol* **526**, 1389-1402 (2018).

61. Yackle, K., *et al.* Breathing control center neurons that promote arousal in mice. *Science* **355**, 1411-1415 (2017).

62. Kocsis, B. Basis for differential coupling between rhythmic discharges of sympathetic efferent nerves. *Am J Physiol* **267**, R1008-1019 (1994).

63. Kocsis, B., Karlsson, T. & Wallin, B.G. Cardiac- and noncardiac-related coherence between sympathetic drives to muscles of different human limbs. *Am J Physiol* **276**, R1608-1616 (1999).

64. Hauer, B.E., Pagliardini, S. & Dickson, C.T. The Reuniens Nucleus of the Thalamus Has an Essential Role in Coordinating Slow-Wave Activity between Neocortex and Hippocampus. *eNeuro* **6** (2019).

65. Totah, N.K., Neves, R.M., Panzeri, S., Logothetis, N.K. & Eschenko, O. The Locus Coeruleus Is a Complex and Differentiated Neuromodulatory System. *Neuron* **99**, 1055-1068 e1056 (2018).

66. Szkudlarek, H.J., Orlowska, P. & Lewandowski, M.H. Light-induced responses of slow oscillatory neurons of the rat olivary pretectal nucleus. *PLoS One* **7**, e33083 (2012).

67. Granata, A.R. & Cohen, M.I. Different types of barosensory synaptic inputs to rostral ventrolateral medulla neurons of the rat. *Brain Res* **998**, 36-47 (2004).

68. Kocsis, B. & Gyimesi-Pelczer, K. Spinal segments communicating resting sympathetic activity to postganglionic nerves of the stellate ganglion. *Am J Physiol* **275**, R400-409 (1998).

69. Vertes, R.P., Colom, L.V., Fortin, W.J. & Bland, B.H. Brainstem sites for the carbachol elicitation of the hippocampal theta rhythm in the rat. *Exp Brain Res* **96**, 419-429 (1993).

70. Sorman, E., Wang, D., Hajos, M. & Kocsis, B. Control of hippocampal theta rhythm by serotonin: role of 5-HT2c receptors. *Neuropharmacology* **61**, 489-494 (2011).

71. Ly, S., Pishdari, B., Lok, L.L., Hajos, M. & Kocsis, B. Activation of 5-HT6 receptors modulates sleep-wake activity and hippocampal theta oscillation. *ACS Chem Neurosci* **4**, 191-199 (2013).

72. Pagliardini, S., Greer, J.J., Funk, G.D. & Dickson, C.T. State-dependent modulation of breathing in urethane-anesthetized rats. *J Neurosci* **32**, 11259-11270 (2012).

73. Jessberger, J., Zhong, W., Brankack, J. & Draguhn, A. Olfactory Bulb Field Potentials and Respiration in Sleep-Wake States of Mice. *Neural Plast* **2016**, 4570831 (2016).

74. Farre, R., Montserrat, J.M. & Navajas, D. Noninvasive monitoring of respiratory mechanics during sleep. *Eur Respir J* **24**, 1052-1060 (2004).

**Acknowledgements.** This work was supported by the National Institute of Mental Health grant R01 MH100820 to BK and a Swedish Government stipend to RM.

**Author contributions**. RM and BK contributed to the experiments, analysis, interpreting the results, and writing the report.

**Competing Interests:** The authors declare no competing interests.